Journal of Power Sources 263 (2014) 296–303

Contents lists available at ScienceDirect

Journal of Power Sources

journal homepage: www.elsevier.com/locate/jpowsour

Preparation and electrochemical performance of La^{3+} and F^- co-doped $Li_4Ti_5O_{12}$ anode material for lithium-ion batteries

Mandi Ji [a], Yunlong Xu [a,*], Zhen Zhao [a], Huang Zhang [a], Dong Liu [b], Chongjun Zhao [a], Xiuzhen Qian [a], Chunhua Zhao [a]

[a] Key Laboratory for Ultrafine Materials of Ministry of Education, Shanghai Key Laboratory of Advanced Polymeric Materials, School of Materials Science and Engineering, East China University of Science and Technology, 130 Meilong Road, Shanghai 200237, PR China
[b] Department of Materials Science and Engineering, University of Texas at Arlington, Arlington, TX 76019, USA

HIGHLIGHTS

- La^{3+}, F^- co-doped $Li_4Ti_5O_{12}$ materials are synthesized via a solid state reaction.
- La^{3+} and F^- ions enter the different sites of the crystal structure of $Li_4Ti_5O_{12}$.
- La^{3+} and F^- co-doping can improve the capacity and maintain the cycling stability.
- $Li_{3.95}La_{0.05}Ti_5O_{11.7}F_{0.3}$ exhibits excellent rate and better cycle performance.

ARTICLE INFO

Article history:
Received 19 January 2014
Received in revised form
27 March 2014
Accepted 11 April 2014
Available online 24 April 2014

Keywords:
$Li_4Ti_5O_{12}$
Co-doping
Conductivity
Rate capability
Low temperature

ABSTRACT

La^{3+} and F^- co-doped $Li_4Ti_5O_{12}$ (LTO) anode materials are synthesized successfully via a solid state reaction. The structure and morphology are characterized by XRD, SEM and EDS. The results indicate that La^{3+} and F^- ions were uniformly dispersed in $Li_4Ti_5O_{12}$ lattice without changing the structure and morphology of $Li_4Ti_5O_{12}$. $Li_{3.95}La_{0.05}Ti_5O_{11.7}F_{0.3}$ (La005-F03) exhibits an outstanding electrochemical performance among all the samples in a potential range from 0.5 to 2.5 V, and delivers a discharge capacity of 103 mAh g^{-1} at 10C rate, whereas the LTO only gives 62.5 mAh g^{-1}. The sample La005-F03 retains a discharge capacity of 170.1 mAh g^{-1} after 100 cycles at 1C rate. The improved electrochemical performance could be attributed to the appropriate co-doping with La^{3+} and F^-, which can increase the amount of Ti^{3+}/Ti^{4+} mixing as charge compensation, leading to the decrease of the charge transfer resistance and improvement of the electronic conductivity and lithium ion diffusion coefficient.

1. Introduction

Recently, spinel $Li_4Ti_5O_{12}$ is attracting more and more attentions as an anode material for advanced electrochemical energy storage devices such as lithium ion batteries [1,2]. The spinel $Li_4Ti_5O_{12}$ has a higher Li insertion voltage (ca. 1.5 V vs. Li^+/Li), which can avoid reduction of electrolyte on the surface of the electrode [3]. On the other hand, the spinel $Li_4Ti_5O_{12}$ is a "zero-strain" insertion material, which has excellent reversibility during lithium insertion/extraction process [4]. These two features make it to be a promising anode material for lithium ion batteries used in the fields of hybrid electric vehicles and large-scale energy storage.

However, $Li_4Ti_5O_{12}$ exhibits poor electronic and lithium ionic conductivities [5–7], thereby limiting itself in high rate charge/discharge application. To improve the conductivities, several effective ways have been proposed, including synthesis of nano-sized $Li_4Ti_5O_{12}$ [8–10], doping with aliovalent ions (V^{5+}, Nb^{5+}, Zn^{3+}, Cr^{3+}, Ni^{2+}, Mg^{2+}, Br^-, F^-) in Li, Ti or O sites [11–18], incorporation of second phase with high electronic conductivity, such as carbon coating layer [19–22], TiN nano-coating layer [23] and TiO_2 nano-coating layer [24].

Carbon-coated $Li_4Ti_5O_{12}$ and nanostructured $Li_4Ti_5O_{12}$ materials appear to be more efficient for improving the high rate capability, due to the enhanced electronic conductivity and the significantly shortened transport paths for both lithium ions and electrons. However, the volumetric energy density of the carbon-coated $Li_4Ti_5O_{12}$ and nanostructured $Li_4Ti_5O_{12}$ is very small because their low packing density results in very poor loading of the active

* Corresponding author. Tel./fax: +86 021 64252019.
E-mail addresses: xiaoxiangzi2009@163.com, xuyunlong@ecust.edu.cn (Y. Xu).

http://dx.doi.org/10.1016/j.jpowsour.2014.04.051
0378-7753/

material in the cell [20]. In addition, the fabrication of nano-sized $Li_4Ti_5O_{12}$ particles and achieving a uniform surface coating around the whole $Li_4Ti_5O_{12}$ particle are still challenges using a solid-state reaction or sol–gel method [20,22]. Therefore doping with aliovalent ions may be the most promising way to strengthen its rate performance. B. Zhang et al. [25] found that Sn-doping can increase the conductivity of $Li_4Ti_5O_{12}$, and thus to improve its rate capability. It also has been reported that La^{3+} doping can improve the electronic conductivity of $Li_4Ti_5O_{12}$, and then lead to the improvement of rate performance [26]. Moreover, Y. L. Qi et al. [17] reported that Br-doped $Li_4Ti_5O_{12}$ exhibits an excellent discharge capacity due to the decreased charge transfer resistance and the enhanced conductivity, thus to improve the rate performance of the $Li_4Ti_5O_{12}$.

As mentioned that both cation doping and anion doping could increase the conductivity of $Li_4Ti_5O_{12}$, we considered if the cation and anion co-doping can further enhance the electrochemical performance, as the so-called "Synergistic Effect". According to the previous studies [26,18], we chose La and F as the dopants and synthesized the La^{3+} and F^- co-doping $Li_4Ti_5O_{12}$ compounds. The effects of La^{3+} and F^- co-doping on the electrochemical performance have been investigated in detail at different operation temperatures.

2. Experimental

2.1. Material preparation

The pristine $Li_4Ti_5O_{12}$, La^{3+} doped $Li_4Ti_5O_{12}$ and La^{3+}/F^- co-doped $Li_4Ti_5O_{12}$ compounds were prepared by a high temperature solid state reaction. The raw materials consisted of Li_2CO_3 (AR, Shanghai Chemical Agents Co. Ltd), anatase TiO_2 (AR, Nanjing High Technology Nano Material Co. Ltd), $La(NO_3)_3\cdot 6H_2O$ (AR, Shanghai Chemical Agents Co. Ltd) and LiF (AR, Aladdin Industrial Inc.) according to the stoichiometric quantities of $Li_4Ti_5O_{12}$, $Li_{3.95}La_{0.05}Ti_5O_{12}$, $Li_{3.95}La_{0.05}Ti_5O_{11.9}F_{0.1}$, $Li_{3.95}La_{0.05}Ti_5O_{11.7}F_{0.3}$ and $Li_{3.95}La_{0.05}Ti_5O_{11.5}F_{0.5}$, respectively. Excess Li was added to compensate for lithium volatilization during the sintering process. The raw materials were mixed by ball milling for 6 h in ethanol slurry, followed by rotary evaporation at 70 °C for 30 min to obtain the precursors. The as-prepared precursor powders were calcined in a tube furnace at 800 °C for 10 h in a flowing argon atmosphere, then annealing to room temperature. The synthesized samples were ground before powder characterization and electrode preparation. These samples were labeled as LTO, La005, La005-F01, La005-F03 and La005-F05, respectively.

2.2. Material characterization

Powder X-ray diffraction (XRD, D/max2550VB3+/PC, Japan) using Cu K_α radiation ($\lambda = 1.54056$ Å) was used to identify the phase composition and crystal lattice parameters of the synthesized samples. The surface morphology of the samples was observed by a scanning electron microscope (SEM, Nova Nano SEM MPE218, FEI). The distribution of the elements of the samples was analyzed by energy dispersive spectrometer, which combined with scanning electron microscopy (SEM, Hitachi S4800, Japan).

2.3. Electrochemical measurements

The synthesized powders were thoroughly mixed with 10% polyvinylidene fluoride (PVDF) and 10% acetylene black (AB) in N-methyl-2-pyrrolidone (NMP). The obtained slurries were then brushed onto silver foils' substrate and dried in a vacuum oven at 120 °C for 12 h, respectively. Lithium foil was used as the counter electrode, and Celgard 2400 microporous polyethylene membrane as the separator. The electrolyte was a mixture of 1 M $LiPF_6$ in ethylene carbonate (EC)/diethyl carbonate (DEC) (1:1 by volume). The cells were assembled in an argon-filled glove box and were left to age for at least 12 h before charge/discharge test. The charge/discharge cycling was performed on a battery test instrument (CT2001A, LAND Battery Program-control Test System, China) over a voltage range of 0.5–2.5 V. The electrochemical behaviors of the individual composite electrodes were characterized by cyclic voltammetry (CV), in coin cells at a scan rate of 0.1 mV s^{-1}, on an Electrochemical Workstation (CHI, 660B, CHENHUA, China). Electrochemical impedance spectroscopies (EIS) of the cells were also conducted on the Electrochemical Workstation (CHI, 660B, CHENHUA, China). The EIS spectra were potentiostatically collected by using a DC potential equal to the open circuit voltage of the cell and an AC oscillation of 5 mV over a frequency range of 10000 Hz–0.01 Hz.

3. Results and discussion

Fig. 1 shows the X-ray diffraction (XRD) patterns of the as-obtained samples synthesized with different La/F molar ratios and the pure sample. The diffraction peaks of all investigated samples are in accordance with the diffraction pattern of the face-centered cubic spinel $Li_4Ti_5O_{12}$ with the Fd-3m space group (JCPDS Card No.49-0207), and no impurity peaks can be detected, indicating that the La^{3+} and F^- ions had entered the lattice of $Li_4Ti_5O_{12}$ without destroying the crystal structure or forming a new phase. However, the lattice parameters of synthesized samples are changed, as shown in Table 1. The standard lattice parameter of $Li_4Ti_5O_{12}$ is 0.8359 nm, and the lattice parameters of synthesized samples LTO, La005, La005-F01, La005-F03 and La005-F05 are 0.8359(5)nm, 0.8367(3)nm, 0.8361(8)nm, 0.8361(1)nm, 0.8360(8) nm, respectively. The changing trend shown on the lattice parameters of synthesized samples is related to the doping amount of the La^{3+} and F^-, and the lattice parameter extends with the doping of La ions, and then reduces with the co-doping of F ions. This suggests that La^{3+} and F^- ions had entered the different sites of the crystal structure and produced adverse lattice distortion.

Fig. 2 shows the crystal structure model of $Li_4Ti_5O_{12}$ built on Materials Studio. Purple spheres denote lithium ions, grey spheres

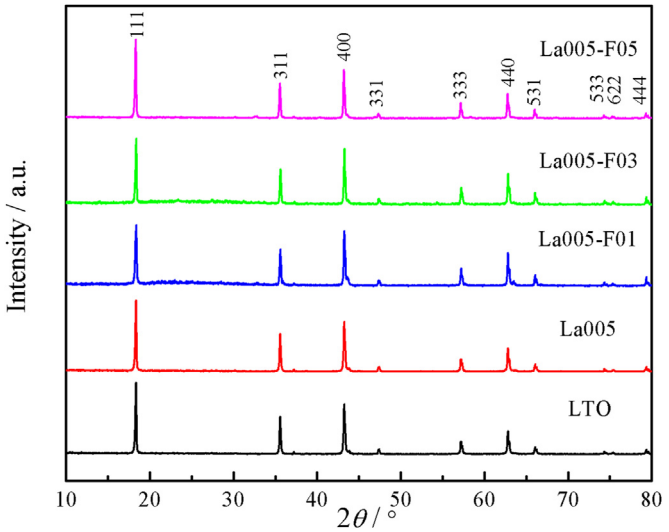

Fig. 1. XRD patterns of the as-obtained samples synthesized with different La/F molar ratios and the pure sample.

Table 1
Lattice parameters of the as-obtained samples.

Sample	a(nm)	b(nm)	c(nm)
$Li_4Ti_5O_{12}$	0.83595	0.83595	0.83595
$Li_{3.95}La_{0.05}Ti_5O_{12}$	0.83673	0.83673	0.83673
$Li_{3.95}La_{0.05}Ti_5O_{11.9}F_{0.1}$	0.83618	0.83618	0.83618
$Li_{3.95}La_{0.05}Ti_5O_{11.7}F_{0.3}$	0.83611	0.83611	0.83611
$Li_{3.95}La_{0.05}Ti_5O_{11.5}F_{0.5}$	0.83608	0.83608	0.83608

denote titanium ions and red spheres denote oxygen ions. The simulated image based on the actual ionic radius. The radii of Li^+, Ti^{4+}, Ti^{3+}, La^{3+}, O^{2-} and F^- ions are as following: $\gamma(Li^+) = 0.076$ nm, $\gamma(Ti^{4+}) = 0.0605$ nm, $\gamma(Ti^{3+}) = 0.067$ nm, $\gamma(La^{3+}) = 0.1032$ nm, $\gamma(O^{2-}) = 0.14$ nm and $\gamma(F^-) = 0.133$ nm, respectively. The difference of radius between La^{3+} and Li^+ or Ti^{4+} or Ti^{3+} are more than that between O^{2-} and F^-. It is well known that many elements can be doped into the 8a Li^+ tetrahedral sites or 16d octahedral sites of $Li_4Ti_5O_{12}$ [27]. So, when La^{3+} ions are doped into the $Li_4Ti_5O_{12}$ lattice individually, La atoms may be doped into the 8a Li^+ tetrahedral site or 16d octahedral site of the $Li_4Ti_5O_{12}$ lattice and induce the lattice distortion due to the difference in ionic radius, which can be reflected in the difference of lattice parameters between sample LTO and sample La005, as shown in Table 1. While La^{3+}, F^- ions are co-doped into the $Li_4Ti_5O_{12}$ lattice, F atoms may be substitute the O atoms due to the similar ionic radius, which can be confirmed by the lattice parameters of the co-doped samples, as shown in Table 1.

Fig. 3 shows the typical scanning electron microscopy (SEM) images of the pristine $Li_4Ti_5O_{12}$ and sample La005-F03. From the images, we can see that the sample is composed of irregular particles, and the particle size is almost in a range of 0.3–1.0 μm. Apparently, doping with La^{3+} and F^- has not changed the morphology of $Li_4Ti_5O_{12}$.

In order to see if the doped elements are uniformly dispersed in $Li_4Ti_5O_{12}$, we analyzed the elemental mapping of sample La005-F03 by Energy Dispersion Spectroscopy (EDS) measurement. Fig. 4a is the SEM image of the tested area, Fig. 4b shows the integral distribution of the element O, Ti, La and F in the tested area, Fig. 4(c–f) exhibit the separate distributions of the different elements O, Ti, La and F in the area, respectively. As presented in Fig. 4(c–f), all these elements have homogeneous distributions, which suggest that the La^{3+} and F^- uniformly doped into $Li_4Ti_5O_{12}$ crystal structure via the high temperature solid-stated reaction.

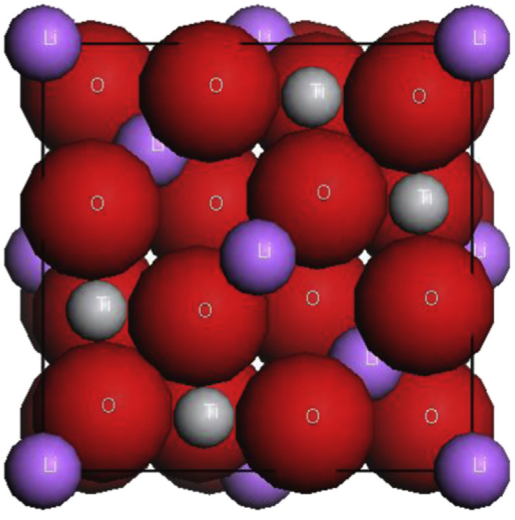

Fig. 2. Crystal structure model of $Li_4Ti_5O_{12}$ built on Materials Studio.

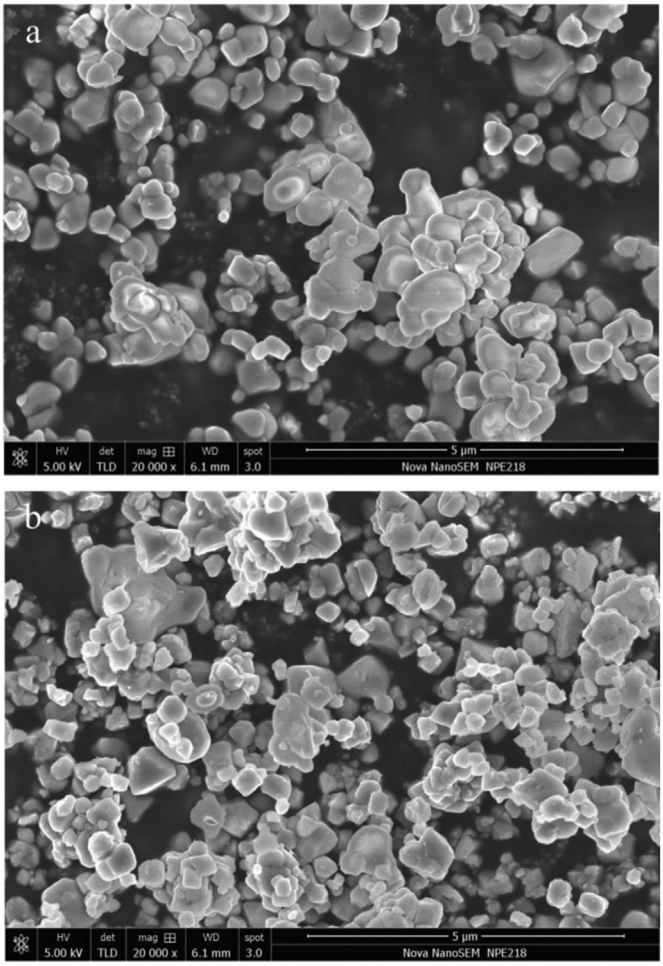

Fig. 3. SEM images of sample (a) LTO and (b) La005-F03.

Fig. 5(a) and (b) show the cycle performance of the as-obtained samples at 1C and 5C rate, respectively. The cut-off voltage is set between 0.5 and 2.5 V. The doped samples show better discharge capacities than the pristine $Li_4Ti_5O_{12}$. Moreover, among all the samples with different doping amounts, the sample La005 presents the highest discharge capacity than others in the first few cycles, however the discharge capacity begins to rapidly decline soon. It may be because the doping of La ions can induce the transition from Ti^{4+} to Ti^{3+} for charge compensation during the charge/discharge process, but $Li_{3.95}La_{0.05}Ti_5O_{12}$ is not stable for lithium ions insertion and extraction owing to the large lattice distortion. The initial discharge capacities of all samples at 1C rate are 155.1, 190.6, 165.8, 180.8 and 173.1 mAh g^{-1}, respectively. And sample La005 and La005-F03 show higher capacities than the theoretical capacity of $Li_4Ti_5O_{12}$ (175 mAh g^{-1}). It is known that almost all the electrochemical energy comes from the reversible redox reactions between trivalent titanium ion (Ti^{3+}) and tetravalent titanium ion (Ti^{4+}) [28]. The improvement of discharge capacity could be attributed to the increasing amount of Ti ions transferred from Ti^{4+} to Ti^{3+} by the doping of La^{3+} for charge compensation and the slight decrease and the stability may be ascribed to the doping of F^- which can reduce the "Ti^{4+}/Ti^{3+}" transition and the lattice distortion. After 100 cycles, the discharge capacities keep 141.4, 151.7, 155.3, 170.1 and 165 mAh g^{-1}, respectively. When testing at a high current density (5C rate), the doped samples still retain more discharge capacities than pristine one except sample La005. The discharge capacities of all samples at 5C rate after 100 cycles are

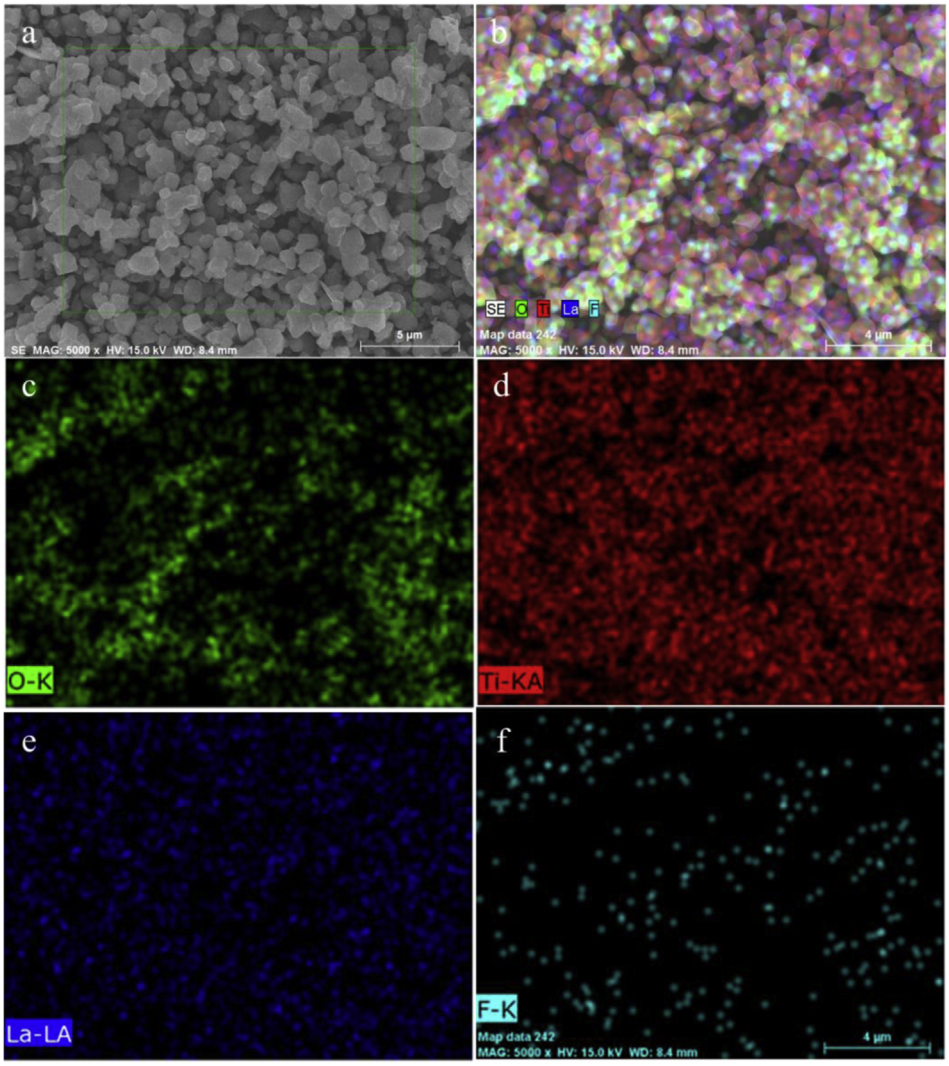

Fig. 4. Elemental mapping for the particles of sample La005-F03.

101, 94.4, 125.8, 135.8 and 131.1 mAh g^{-1}, respectively. Fig. 5(a) and (b) indicate that the dopant La ions can improve the discharge capacity of $Li_4Ti_5O_{12}$ but show a relatively poor stability, while the co-doping of La and F can simultaneously improve the discharge capacity and maintain the cycling stability, as the so-called "Complementary Effect". Furthermore, sample La005-F03 presents the highest discharge capacity and best cycling stability.

Fig. 6 displays the initial charge/discharge curves of sample LTO and La005-F03 at different rates. Each charge/discharge curve shows a flat voltage plateau at around 1.55 V (vs. Li^+/Li), which is the characteristic of two-phase reaction [29].The capacities of LTO discharged at 0.2C, 1C, 2C, 5C, 10C rate are 174.7, 155, 146, 100, 62.5 mAh g^{-1}, respectively. Correspondingly, sample La005-F03 delivers higher discharge capacities, especially at high rates. Sample La005-F03 delivers a discharge capacity of 193 mAh g^{-1} at 0.2C rate, 175 mAh g^{-1} at 1C, 167 mAh g^{-1} at 2C, 131 mAh g^{-1} at 5C and 103 mAh g^{-1} at 10C. The differences of the discharge capacities between sample La005-F03 and LTO at different rates are 18.3, 20, 21, 31, 40.5 mAh g^{-1}, which mean La^{3+} and F^- co-doping can improve the rate performance of $Li_4Ti_5O_{12}$. Comparing Fig. 5 with Fig. 6, we can find an irreversible capacity fading after first discharge, the reason could be explained that the SEI film had been formed at the surface of $Li_4Ti_5O_{12}$ electrode when the cut-off voltage is blow 1.0 V [30].

To further investigate the electrochemical behaviors of the five samples, EIS measurements were performed as seen in Fig. 7. All the electrochemical impedance spectroscopies were carried out at the fully charged state at 25 °C after 100 cycles. The EIS spectra all consist of a semicircle in the high frequency range and a sloping line in the low-frequency range. The EIS spectra are fitted using an equivalent circuit as shown in Fig. 7. The symbols R_e and R_{ct} in the equivalent circuit represent the electrolyte resistance and the charger-transfer resistance at the electrolyte/electrode interface, respectively. CPE represents the double-layer capacitance, and σ_w is referred to the Warburg impedance, which is related to the Li-ions diffusion in the bulk electrode.

The EIS spectra are fitted using ZsimpWin software and the fitting results are listed in Table 2. The R_{ct} values of the LTO, La005, La005-F01, La005-F03 and La005-F05 samples are 260.3, 201.8, 126.4, 42.2 and 126Ω, respectively. The La005-F03 electrode exhibits much smaller R_{ct} than the others. This should be ascribed to the increasing electronic conductivity by the modest co-doping of La^{3+} and F^- ions. The values of the charger-transfer resistance are in good agreement with the results shown in Fig. 5. That is, the higher the charger-transfer resistance of the $Li_4Ti_5O_{12}$ cell is, the more dramatically the capacity decreases.

The inclined line is attributed to the diffusion of the lithium ions into the bulk of the electrode material, the so-called Warburg

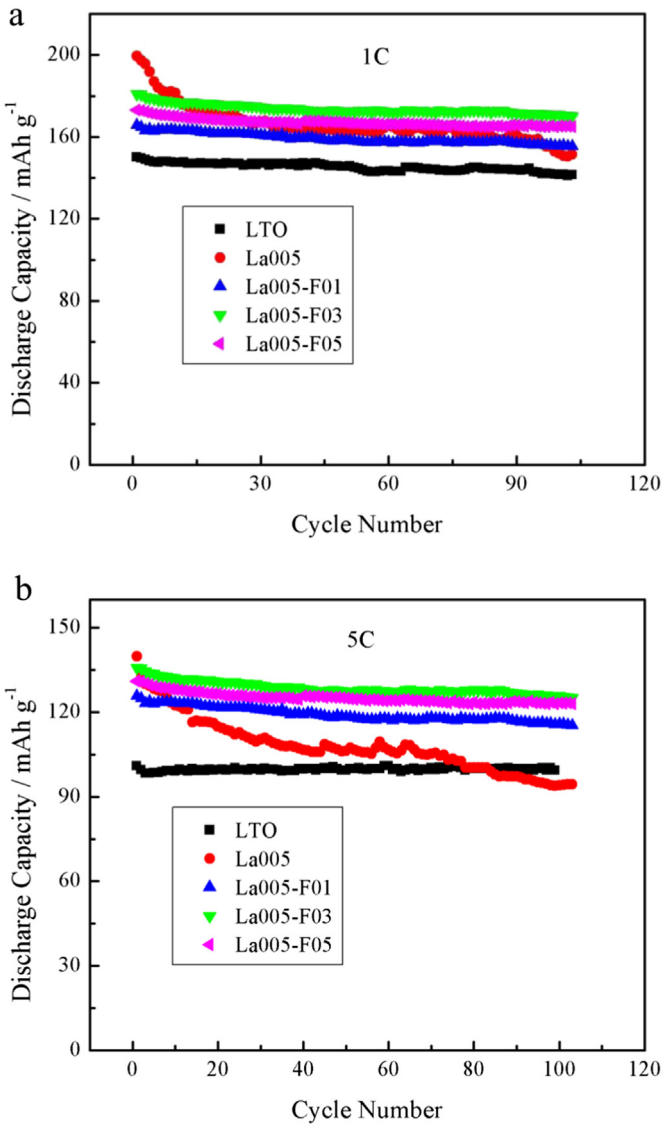

Fig. 5. Cycle performance curves of the as-obtained samples at different rates: (a) 1C rate; (b) 5C rate.

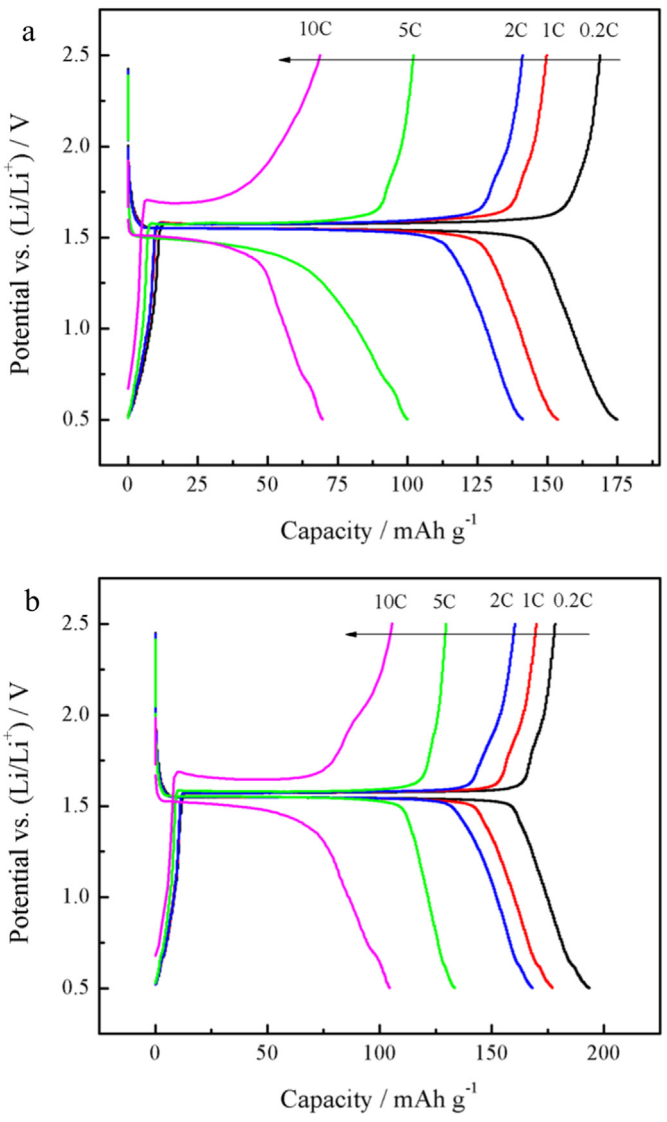

Fig. 6. Initial charge and discharge curves at different rate at room temperature: (a) pure $Li_4Ti_5O_{12}$ and (b) sample La005-F03.

diffusion. The Warburg coefficient σ_w can be obtained by Eq. (1) [26]:

$$Z_{re} = R_e + R_{ct} + \sigma_w \omega^{-1/2} \quad (1)$$

where Z_{re} is the real part of the impedance, R_e is the resistance of the electrolyte, R_{ct} is the charge transfer resistance and ω is the angular frequency in the low frequency region. Both R_e and R_{ct} are kinetics parameters independent of frequency. And ω is the slope for the plot of Z_{re} vs. the reciprocal root square of the lower angular frequency ($\omega^{-1/2}$).

The plot of Z_{re} vs. the reciprocal root square of the lower angular frequencies ($\omega^{-1/2}$) for all the samples is shown in Fig. 8. In the plots, the symbols and solid lines represent the experimental points and fitting results, respectively. The slope of fitted line is Warburg coefficient σ_w, as shown in Table 2. The σ_w values of the samples are 51.56, 47.31, 3.84, 1.87 and 8.21 Ω cm^2 $s^{-1/2}$, respectively. It can be seen that the Warburg coefficient σ_w for the sample La005-F03 is the lowest compared with others. As a consequence, the sample of La005-F03 shows the highest lithium ion diffusion coefficient.

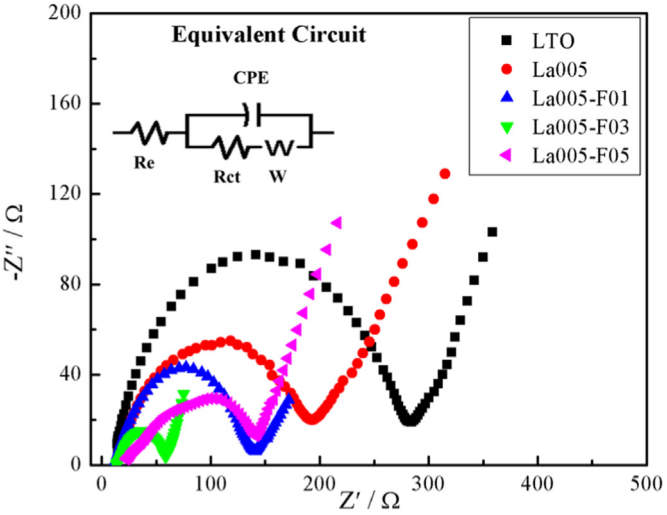

Fig. 7. EIS spectra of the electrodes in the frequency range between 0.01 Hz and 100 kHz.

Table 2
Impedance parameters of the as-obtained samples.

Sample	$R_e(\Omega)$	$R_{ct}(\Omega)$	$\sigma_w(\Omega\ cm^2\ s^{-1/2})$	$\sigma(S\ cm^{-1})$	$i^0(mA\ cm^{-2})$	$D(cm^2\ s^{-1})$
LTO	11.33	260.3	51.56	1.25×10^{-5}	3.29×10^{-5}	3.64×10^{-15}
La005	22.9	201.8	47.31	1.61×10^{-5}	4.24×10^{-5}	4.32×10^{-15}
La005-F01	12.43	126.4	3.84	2.57×10^{-5}	6.78×10^{-5}	6.55×10^{-13}
La005-F03	14.64	42.2	1.87	7.7×10^{-5}	2.03×10^{-4}	2.76×10^{-12}
La005-F05	21.47	124	8.21	2.62×10^{-5}	6.91×10^{-5}	1.43×10^{-13}

R_e: electrolyte resistance; R_{ct}: charge transfer resistance; σ_w: Warburg impedance; σ: conductivity; i^0: the exchange current density; D: diffusion coefficient of the lithium ions.

The conductivity values (σ) are calculated from Eq. (2) [26]:

$$\sigma = \frac{1}{R_{ct}} \frac{t}{A} \tag{2}$$

where R_{ct} is the charger-transfer resistance, t is the thickness of the cathode and A is the area of the electrode surface. The σ values of the samples are 1.25×10^{-5}, 1.61×10^{-5}, 2.57×10^{-5}, 7.7×10^{-5} and 2.62×10^{-5} S cm^{-1}, respectively. Although the conductivity of La005-F03 shows only a little higher than those of others, the capacity and cycle performance are much better.

Also, the values of the exchange current density (i^0) are calculated from Eq. (3) [31]:

$$i^0 = \frac{RT}{nFR_{ct}} \tag{3}$$

where R is the gas constant (8.314 J mol^{-1} K^{-1}), T is the absolute temperature in Kelvin (298.15 K), n is the number of electrons transferred per molecule during the intercalation (for $Li_4Ti_5O_{12}$, $n = 3$), F is the Faraday's constant (96,500 C mol^{-1}) and R_{ct} is the charge transfer resistance.

The exchange current density is a parameter to indicate the reversibility of the electrode. The greatest value of i^0 is obtained with the sample La005-F03 (ca. 2.03×10^{-4}), corresponding to an increase by about 1 order of magnitude compared with the pure $Li_4Ti_5O_{12}$, implying its better reversibility than others.

In addition, the diffusion coefficient values of the lithium ions (D_{Li}^{+}) can be obtained from Eq. (4) [26]:

$$D_{Li^+} = \frac{R^2T^2}{2A^2n^4F^4C^2\sigma_w^2} \tag{4}$$

where R is the gas constant (8.314 J mol^{-1} K^{-1}), T is the absolute temperature in Kelvin (298.15 K), A is the area of the electrode surface, n is the number of electrons transferred per molecule during the intercalation and is 3 for $Li_4Ti_5O_{12}$, F is the Faraday's constant (96,500 C mol^{-1}), C is the concentration of lithium ion in solid (4.37×10^{-3} mol cm^{-3}) [26,31] and σ_w is the Warburg coefficient, ρ is density of the synthesized materials, M is molecular weight of $Li_4Ti_5O_{12}$.

The D_{Li}^{+} parameters of the synthesized materials obtained from EIS are recorded in Table 2. The D_{Li}^{+} values of the samples are 3.64×10^{-15}, 4.32×10^{-15}, 6.55×10^{-13}, 2.76×10^{-12} and 1.43×10^{-13} cm^2 s^{-1}, respectively. It can be observed that the diffusion coefficient values of the lithium ions (D_{Li}^{+}) for the sample La005-F03 is the highest compared with others. The enhancement of the diffusion coefficient may be mainly attributed to the doping of La^{3+} and F^- ions, which can decrease the amount of active titanium ions (Ti^{4+}) lead to the increasing quantities of Ti^{3+}.

Fig. 9 shows the CV curves of the sample LTO and La005-F03 tested between 0.5 and 2.5 V at a scan rate of 0.1 mV s^{-1} at 25 °C. The CV curves present a similar pair of redox peaks, which correspond to the reversible phase transition between $Li_4Ti_5O_{12}$ and $Li_7Ti_5O_{12}$. The oxidation peaks are at about 1.7 V (anodic delithiation) and the reduction peaks are at 1.4 V (cathodic lithiation) can be attributed solely to the successive oxidation/reduction reactions of the Ti^{3+}/Ti^{4+} couple in the cubic structure, compensated by lithium deinsertion/insertion. It can be observed

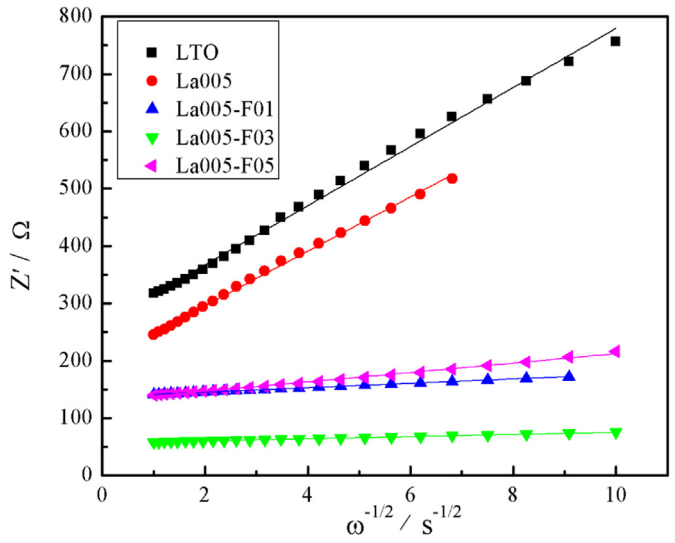

Fig. 8. The relationship between Z′ and $\omega^{-1/2}$ at low frequency for different samples.

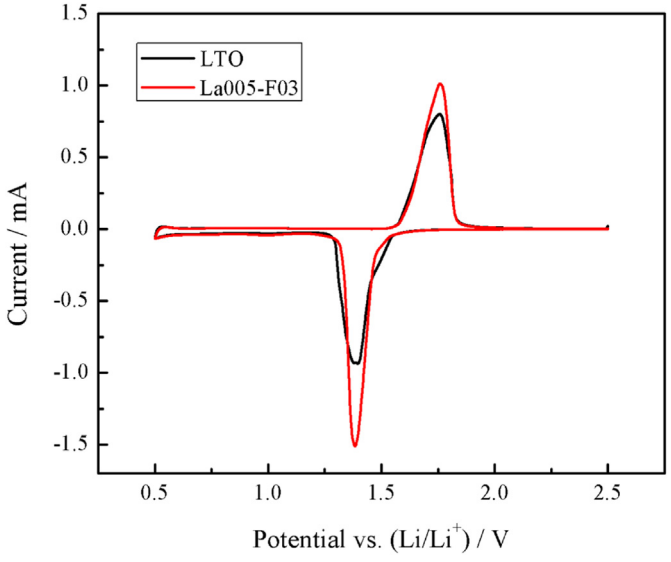

Fig. 9. Cyclic voltammetry(CV) of the sample LTO and La005-F03.

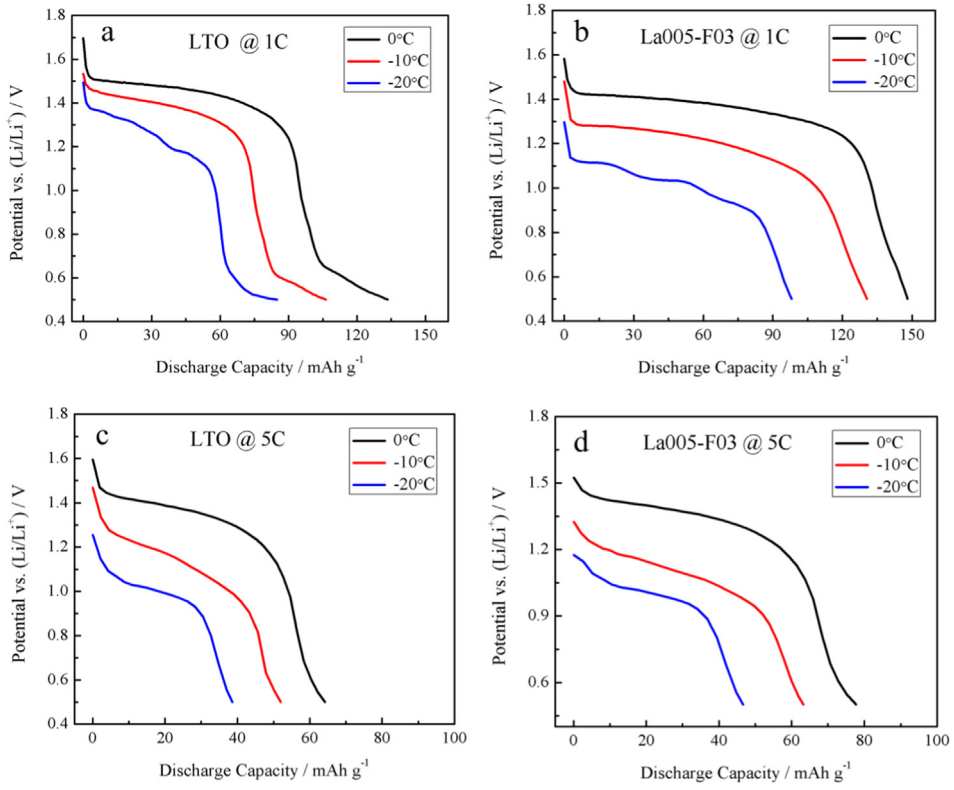

Fig. 10. Discharge curves at different rate under low temperatures from 0 °C to −20 °C.

that the co-doped $Li_4Ti_5O_{12}$ has the highest intensity of both the oxidation and reduction peaks compared with those of the pure $Li_4Ti_5O_{12}$, which indicate that the dopant La and F. does not change the electrochemical reaction process of $Li_4Ti_5O_{12}$ in this voltage range, but increases the charge/discharge capacity of $Li_4Ti_5O_{12}$, which is in accord with the discharge curves.

For practical application, the lithium-ion batteries may often be used in low-temperature environment, especially as power sources

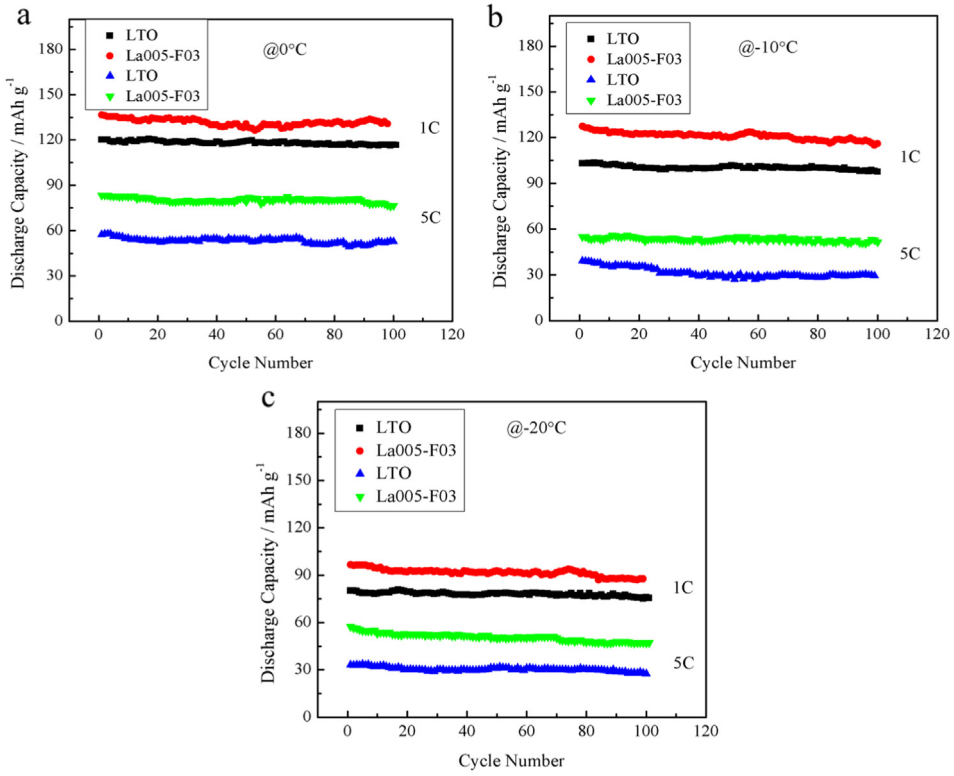

Fig. 11. Cycle performance curves of the samples at different temperatures from 0 °C to −20 °C.

for electric or electric-hybrid vehicles. With the drop of operation temperature, both the surface reaction kinetics and the rate of charge (lithium-ion and electron) diffusion inside the electrode bulk are slowed down. Fig. 10 presents the discharge curves of sample LTO and sample La005-F03 at different rates under different temperatures from 0 °C to −20 °C. Evidently, the capacities significantly decline in comparison with those at 25 °C, especially at high rates, due to the decrease of the surface reaction kinetics and lithium diffusion in the electrode. Apparently, the co-doped sample shows beneficial effect on inhibiting capacity fading. At 0 °C, sample La005-F03 delivers a capacity of 149 mAh g^{-1} at 1C rate, while sample LTO presents 135 mAh g^{-1}. Even at 5C rate, sample La005-F03 still carries out a capacity of 78 mAh g^{-1}, whereas the LTO only gives 63 mAh g^{-1}. When tested at −20 °C, the discharge capacities of the two samples become much smaller than those tested at 0 °C. The capacity of La005-F03 at 1C rate can approximately reach 100 mAh g^{-1}, while LTO gives less than 90 mAh g^{-1}. Comparing the capacities of sample LTO with La005-F03 under different temperatures, we know that the appropriate La^{3+} and F^- co-doping can improve the low temperature performance of $Li_4Ti_5O_{12}$ due to the increased electronic and ionic conductivity.

Fig. 11 shows the comparison of the cycle performance of the pristine and co-doped $Li_4Ti_5O_{12}$ at 1C and 5C rates under different temperatures from 0 °C to −20 °C. It's obvious that the capacities of the two samples are sensitive to the decreasing of the tested environmental temperature. At 0 °C, sample La005-F03 presents a capacity of more than 135 mAh g^{-1} after 100 cycles at 1C rate, while sample LTO only gives 120 mAh g^{-1}. When tested at 5C rate, the differences become more apparent, which suggest that the co-doping of La^{3+} and F^- can remarkably improve the rate capability. When tested at −10 °C, both sample LTO and sample La005-F03 have the further reducing of the discharge capacities. Sample LTO only shows a discharge capacity of 100 mAh g^{-1} after 100 cycles at 1C rate, while sample La005-F03 still retain a capacity of 120 mAh g^{-1}. Even at 5C rate, sample La005-F03 still retain a capacity close to 60 mAh g^{-1}. However, when operated at −20 °C, both LTO and La005-F03 show the discharge capacities lower than 100 mAh g^{-1} at 1C rate, which means the surface reaction kinetics and lithium diffusion in the electrode were declined severely. All the results suggest that the co-doping of La^{3+} and F^- can enhance the electrochemical performance of $Li_4Ti_5O_{12}$ at low temperatures.

4. Conclusions

The La^{3+} and F^- co-doped $Li_4Ti_5O_{12}$ material was successfully synthesized by a solid-state reaction. The La^{3+} and F^- ions had entered the different sites of the crystal structure of $Li_4Ti_5O_{12}$ and produced adverse lattice distortion. The rate cyclic performance of $Li_4Ti_5O_{12}$ can be markedly improved by La^{3+}, F^- co-doping. It can be explained by the fact that the relatively higher conductivity and lithium diffusion coefficient would help to release the stresses generated by the repetitive Li ions intercalation, and then reduce the electrochemical polarization during high rate charge/discharge process. The appropriate La^{3+} and F^- co-doping can not only improve the discharge capacity but also maintain the cycling stability, as the so-called "Complementary Effect". Moreover, the co-doping of La^{3+} and F^- can enhance the electrochemical performance of $Li_4Ti_5O_{12}$ at low temperatures. From the overall performance point of view, sample La005-F03 shows the best electrochemical performance among all samples, which suggests the La^{3+} and F^- co-doped $Li_4Ti_5O_{12}$ material is a promising anode material for lithium ion batteries.

Acknowledgments

This work is supported by Shanghai Leading Academic Discipline Project (B502), Shanghai Nanotechnology Special Foundation (No. 11nm0500900) and Shanghai Key Laboratory Project (08DZ2230500).

References

[1] M. Armand, J.M. Tarascon, Nature 451 (2008) 652.
[2] K. Zaghib, M. Dontigny, A. Guerfi, P. Charest, I. Rodrigues, A. Mauger, C.M. Julien, J. Power Sources 196 (2011) 3949–3954.
[3] I. Belharouak, Y.K. Sun, W. Lu, K.J. Amine, J. Electrochem. Soc. 154 (2007) A1083–A1087.
[4] K. Ariyoshi, R. Yamato, T. Ohzuku, Electrochim. Acta 51 (2005) 1125–1129.
[5] Z.M. Liu, N.Q. Zhang, Z.J. Wang, K.N. Sun, J. Power Sources 205 (2012) 479–482.
[6] X. Li, M.Z. Qu, Y.J. Huai, Z.L. Yu, Electrochim. Acta 55 (2010) 2978–2982.
[7] Pierre Kubiak, Aurélie Garcia, Manfred Womes, Laurent Aldon, Josette Olivier-Fourcade, Pierre-Emmanuel Lippens, Jean-Claude Jumas, J. Power Sources 119–121 (2003) 626–630.
[8] L. Cheng, J. Yan, G.N. Zhu, J.Y. Luo, C.X. Wang, Y.Y. Xia, J. Mater. Chem. 20 (2010) 595–602.
[9] Mi Ru Jo, Ki Min Nam, Youngmin Lee, Kyeongse Song, Joon T. Park, Yong-Mook Kang, Chem. Commun. 47 (2011) 11474–11476.
[10] Y.F. Tang, F.Q. Huang, W. Zhao, Z.Q. Liu, D.Y. Wan, J. Mater. Chem. 22 (2012) 11257–11260.
[11] T.F. Yi, J. Shu, Y.R. Zhu, X.D. Zhu, R.S. Zhu, A.N. Zhou, J. Power Sources 195 (2010) 285–288.
[12] B.B. Tian, H.F. Xiang, Le Zhang, H.H. Wang, J. Solid State Electrochem. 16 (2012) 205–211.
[13] T.F. Yi, H.P. Liu, Y.R. Zhu, L.J. Jiang, Y. Xie, R.S. Zhu, J. Power Sources 215 (2012) 258–265.
[14] H. Song, S.W. Yun, H.H. Chun, M.G. Kim, K.Y. Chung, H.S. Kim, B.W. Cho, Y.T. Kim, Energy Environ. Sci. 5 (2012) 9903–9913.
[15] C.F. Lin, M.O. Lai, Li Lua, H.H. Zhou, Y.L. Xin, J. Power Sources 244 (2013) 272–279.
[16] S.Z. Ji, J.Y. Zhang, W.W. Wang, Y. Huang, Z.R. Feng, Z.T. Zhang, Z.L. Tang, Mater. Chem. Phys. 123 (2010) 510–515.
[17] Y.L. Qi, Y.D. Huang, D.Z. Jia, S.J. Bao, Z.P. Guo, Electrochim. Acta 54 (2009) 4772–4776.
[18] Z. Zhao, Y.L. Xu, M.D. Ji, H. Zhang, Electrochim. Acta 109 (2013) 645–650.
[19] Alok Kumar Rai, Jihyeon Gim, Sung-Won Kang, Vinod Mathew, Ly Tuan Anh, Jungwon Kang, Jinju Song, Baboo Joseph Paul, Jaekook Kim, Mater. Chem. Phys. 136 (2012) 1044–1051.
[20] H.G. Jung, S.T. Myung, C.S. Yoon, S.B. Son, K.H. Oh, K. Amine, B. Scrosati, Y.K. Sun, Energy Environ. Sci. 4 (2011) 1345.
[21] N. Jayaprakash, Surya S. Moganty, Xiong Wen Lou, Lynden A. Archer, Appl. Nanosci. 1 (2011) 7–11.
[22] L.F. Shen, C.Z. Yuan, H.J. Luo, X.G. Zhang, L. Chen, H.S. Li, J. Mater. Chem. 21 (2011) 14414–14416.
[23] Z.N. Wan, R. Cai, S.M. Jiang, Z.P. Shao, J. Mater. Chem. 22 (2012) 17773–17781.
[24] Y.Q. Wang, L. Gu, Y.G. Guo, H. Li, X.Q. He, Susumu Tsukimoto, Yuichi Ikuhara, L.-J. Wan, J. Am. Chem. Soc. 134 (2012) 7874–7879.
[25] B. Zhang, Z.D. Huang, Sei Woon Oh, Jang-Kyo Kim, J. Power Sources 196 (2011) 10692–10697.
[26] T.F. Yi, Y. Xie, Q.J. Wu, H.P. Liu, L.J. Jiang, M.F. Ye, R.S. Zhu, J. Power Sources 214 (2012) 220–226.
[27] Y. J Sha, T. Yuan, B. Zhao, R. Cai, H.T. Wang, Z.P. Shao, J. Power Sources 231 (2013) 177–185.
[28] T.F. Yi, Yi Xie, J. Shu, Z. Wang, C.B. Yue, R.S. Zhu, H.B. Qiao, J. Electrochem. Soc. 158 (2011) A266–A274.
[29] Andreas Laumann, Hans Boysen, Martin Bremholm, K. Thomas Fehr, Markus Hoelzel, Michael Holzapfel, Chem. Mater. 23 (2011) 2753–2759.
[30] Ge Ji, Yue Ma, Bo Ding, Jim Yang Lee, Chem. Mater. 24 (2012) 3329–3334.
[31] S.L. Chou, J.Z. Wang, H.K. Liu, S.X. Dou, J. Phys. Chem. C 115 (2011) 16220–16227.